

Parity-detection-based Mach-Zehnder interferometry with coherent and non-Gaussian squeezed vacuum states as inputs

Chandan Kumar ^{1,*} Rishabh ^{2,†} Mohak Sharma,^{1,‡} and Shikhar Arora ^{1,3,§}

¹*Department of Physical Sciences, Indian Institute of Science Education and Research Mohali,
Sector 81 SAS Nagar, Punjab 140306, India*

²*Department of Physics and Astronomy, University of Calgary, Calgary, Alberta, Canada T2N1N4*

³*Department of Physics, University of Illinois at Chicago, Illinois 60607, USA*



(Received 22 March 2023; revised 26 June 2023; accepted 29 June 2023; published 7 July 2023)

We theoretically explore the advantages rendered by non-Gaussian operations in phase estimation using a parity-detection-based Mach-Zehnder interferometer, with one input being a coherent state and the other being a non-Gaussian squeezed vacuum state (SVS). We consider a realistic model to perform three different non-Gaussian operations, namely, photon subtraction, photon addition, and photon catalysis on a single-mode SVS. We start by deriving the Wigner function of the non-Gaussian SVSs, which is then utilized to derive the expression for the phase sensitivity. The analysis of the phase sensitivity reveals that all three different non-Gaussian operations can enhance the phase sensitivity under suitable choices of parameters. We also consider the probabilistic nature of these non-Gaussian operations, the results of which reveal the single-photon addition to be the optimal operation. Further, our analysis also enables us to identify the optimal squeezing of the SVS and the transmissivity of the beam splitter involved in the implementation of the non-Gaussian operations.

DOI: [10.1103/PhysRevA.108.012605](https://doi.org/10.1103/PhysRevA.108.012605)

I. INTRODUCTION

The Mach-Zehnder interferometer (MZI) is the most commonly employed optical instrument in phase measurement [1,2]. If the input beams to the MZI are classical sources, the phase sensitivity is bounded by the shot-noise limit (SNL) [3]. To improve the phase sensitivity, quantum resources such as NOON states, twin Fock states, and squeezed states have been employed. These quantum resources enable the phase sensitivity to go beyond the SNL and reach the Heisenberg limit [4–9].

The maximum squeezing that can be achieved experimentally is bounded [10], which leads to a limited enhancement in the phase sensitivity. To overcome this drawback, one can resort to non-Gaussian (NG) operations such as photon subtraction (PS), photon addition (PA), and photon catalysis (PC). It has already been shown that NG operations can be beneficial in quantum teleportation [11–18], quantum key distribution [19–23], quantum illumination [24], and quantum metrology [25–31].

In particular, Ref. [32] showed that the phase sensitivity of a parity-detection-based MZI at a fixed squeezing could be enhanced when the inputs were a coherent state and an ideal photon-subtracted squeezed vacuum state (SVS) as compared to the case when a coherent state and a SVS were employed as the inputs [33].

In this article, we extend the analysis of Ref. [32] to a wider class of NG states. To generate these NG states, we perform three distinct NG operations, namely, PS, PA, and PC, on SVSs. We implement these NG operations via a realistic model based on multiphoton Fock states, photon-number-resolving detectors, and beam splitters [Fig. 1]. This leads to the generation of three distinct families of states, namely, photon-subtracted SVSs (PSSVSs), photon-added SVSs (PASVSs), and photon-catalyzed SVSs (PCSVSs), which we collectively term as “NGSVSs.”

We then evaluate the Wigner function of these NGSVSs, where the free parameters include the input Fock state, the detected Fock state, and the transmissivity of the beam splitter involved in the implementation of the NG operation. By suitably choosing the input Fock state and the detected Fock state, we can perform PS, PA, or PC operations on SVSs. The Wigner function is then utilized to evaluate the expression of the phase sensitivity for the parity-detection-based MZI.

We analyze the behavior of the phase sensitivity of NGSVSs as a function of different parameters. The analysis reveals that all three NG operations can lead to a significant enhancement under suitable choices of parameters. Further, we take the probabilistic nature of NG operations into account in our analysis, which reveals that the single-photon-added SVS is the optimal state.

It should also be noted that the PS operation considered in Ref. [32] is implemented by the annihilation operator \hat{a} , which is nonphysical. In contrast, our realistic scheme for the implementation of NG operations can be realized with current technologies, including the multiphoton Fock state [34–38] and photon-number-resolving detectors [39–41]. We would like to point out that this realistic model invariably

*chandan.quantum@gmail.com

†rishabh1@ucalgary.ca

‡mohak.quantum@gmail.com

§shikhar.quantum@gmail.com

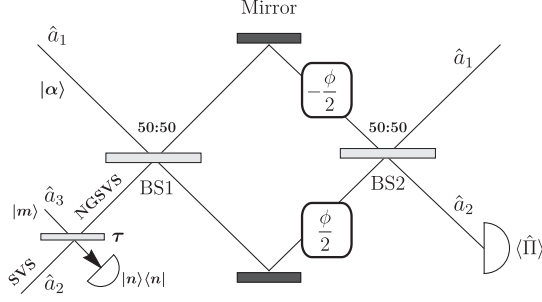


FIG. 1. Schematic diagram for the implementation of NG operations on a SVS followed by a parity-detection-based MZI. The SVS and the ancilla Fock state $|m\rangle$ are combined using a beam splitter of transmissivity τ , and subsequently, detection of n photons in the ancilla output mode heralds the generation of NGSVSs. A coherent state and the NGSVSs serve as the resource states of the MZI for the estimation of the introduced phases.

enhances the complexity of our calculation. Further, the phase sensitivity expression derived here is quite general and special cases investigated in Refs. [32,42] can be obtained in the appropriate limit. Furthermore, the realistic scheme enables us to consider the probabilistic nature of the involved NG operations.

The rest of the paper is structured as follows. In Sec. II, we derive the phase sensitivity expression for the parity-measurement-based MZI with a coherent state and NGSVSs as the two inputs. Section III contains the analysis of the phase sensitivity enhancement using NGSVSs and Sec. IV is dedicated to finding out the optimal NG operation for phase estimation. We summarize our main results and provide directions for future research in Sec. V. In Appendix A, we have provided a detailed calculation of the Wigner distribution function of NGSVSs.

II. PARITY-MEASUREMENT-BASED PHASE ESTIMATION

Consider the setup of a lossless MZI shown in Fig. 1, which consists of two 50:50 beam splitters and two phase shifters. While one of the input states is a coherent state, the other input state is generated by performing different NG operations on a SVS, as depicted in the lower left-hand corner of Fig. 1. An unknown phase ϕ is introduced via the two phase shifters, and we aim to estimate this unknown phase by parity detection on the output mode \hat{a}_2 . The Wigner distribution function of the coherent state $|\alpha\rangle$ can be written as [43]

$$W_{|\alpha\rangle}(\xi_1) = (\pi)^{-1} \exp[-(q_1 - d_x)^2 - (p_1 - d_p)^2], \quad (1)$$

where $\xi_1 = (q_1, p_1)^T$ and $\alpha = (d_x + id_p)/\sqrt{2}$. To implement the NG operations, we mix the SVS and the ancilla Fock state $|m\rangle$ via a beam splitter of transmissivity τ . A photon-number-resolving detector is used to perform a conditional measurement of n photons on the ancilla output mode, which signals the generation of NGSVSs.

For convenience, we employ a phase-space formalism, specifically the Wigner distribution function, for calculations. While stepwise calculation for the derivation of the Wigner distribution function of the NGSVSs is provided in Appendix A, here we provide the final expression. The Wigner

distribution function of the NGSVSs turns out to be [given in Eq. (A17) of Appendix A]

$$W^{\text{NG}}(\xi_2) = \frac{\hat{F}_1 \exp\left(\frac{w_1^2 q_2 + w_2^2 p_2 + u^T M_1 u + u^T M_2}{-w_1 w_2}\right)}{P^{\text{NG}} \sqrt{w_1 w_2}}, \quad (2)$$

where $w_{1,2} = \cosh r \pm \tau \sinh r$ and $\mathbf{u} = (u_1, v_1, u_2, v_2)^T$ represents the column vector. Further,

$$\hat{F}_1 = \frac{(-2)^{m+n}}{\pi m! n!} \frac{\partial^m}{\partial u_1^m} \frac{\partial^m}{\partial v_1^m} \frac{\partial^n}{\partial u_2^n} \frac{\partial^n}{\partial v_2^n} \{\bullet\}_{u_1=v_1=0, u_2=v_2=0} \quad (3)$$

represents the differential operator. The explicit forms of the matrices M_1 and M_2 are provided in Eqs. (A13) and (A14) of Appendix A. The success probability of the NG operations, P^{NG} , is given by [Eq. (A15) of Appendix A]

$$P^{\text{NG}} = \int d^2 \xi_2 \tilde{W}_A^{\text{NG}} = \frac{\pi \hat{F}_1}{\sqrt{w_1 w_2}} \exp\left(\frac{\mathbf{u}^T M_3 \mathbf{u}}{-4w_1 w_2}\right), \quad (4)$$

where the matrix M_3 is given in Eq. (A16) of Appendix A. Different NG operations on SVSs can be implemented by fixing the input Fock state and the detected number of photons. We can perform PS, PA, or PC operations on SVSs under the condition $m < n$, $m > n$, or $m = n$, respectively. In this article, we set $m = 0$ and $n = 0$ for PS and PA operations, respectively. These NG operations convert the SVS state from Gaussian to non-Gaussian.

The derived Wigner distribution function of the SVS (2) is quite general and the Wigner distribution function of special states can be obtained in different limits. For example, the Wigner distribution function of the ideal PSSVSs can be obtained in the limit $\tau \rightarrow 1$ with $m = 0$. The ideal PSSVSs are represented by $\mathcal{N}_s \hat{a}^n |\text{SVS}\rangle$, where \mathcal{N}_s is the normalization factor. Similarly, the Wigner distribution function of the ideal PASVSs can be obtained in the limit $\tau \rightarrow 1$ with $n = 0$. The ideal PASVSs are represented by $\mathcal{N}_a \hat{a}_2^{\dagger m} |\text{SVS}\rangle$, where \mathcal{N}_a is the normalization factor. Finally, the Wigner distribution function of the SVS can be obtained in the limit $\tau \rightarrow 1$ with $m = n$.

For the purpose of ease in the description of the collective action of the MZI, we consider the Schwinger representation of the SU(2) algebra [44]. In terms of the annihilation and creation operators of the input modes, the generators of the SU(2) algebra turn out to be

$$\begin{aligned} \hat{J}_1 &= \frac{1}{2}(\hat{a}_1^\dagger \hat{a}_2 + \hat{a}_1 \hat{a}_2^\dagger), \\ \hat{J}_2 &= \frac{1}{2i}(\hat{a}_1^\dagger \hat{a}_2 - \hat{a}_1 \hat{a}_2^\dagger), \\ \hat{J}_3 &= \frac{1}{2}(\hat{a}_1^\dagger \hat{a}_1 - \hat{a}_2^\dagger \hat{a}_2). \end{aligned} \quad (5)$$

These generators are also known as angular momentum operators and satisfy the commutation relations $[J_i, J_j] = i\epsilon_{ijk} J_k$. The unitary operators acting on the Hilbert space corresponding to the first and the second beam splitters are given by $e^{-i(\pi/2)\hat{J}_1}$ and $e^{i(\pi/2)\hat{J}_1}$, respectively. The combined action of the two phase shifters is represented by the unitary operator $e^{i\phi\hat{J}_3}$. Therefore, the total action of the MZI is represented as a product of the unitary operators as follows:

$$U(S_{\text{MZI}}) = e^{-i(\pi/2)\hat{J}_1} e^{i\phi\hat{J}_3} e^{i(\pi/2)\hat{J}_1} = e^{-i\phi\hat{J}_2}. \quad (6)$$

The corresponding symplectic matrix S_{MZI} transforming the phase-space variables $(\xi_1, \xi_2)^T$ turns out to be

$$S_{\text{MZI}} = \begin{pmatrix} \cos(\phi/2) \mathbb{1} & -\sin(\phi/2) \mathbb{1} \\ \sin(\phi/2) \mathbb{1} & \cos(\phi/2) \mathbb{1} \end{pmatrix}. \quad (7)$$

The evolution of the Wigner distribution function due to S_{MZI} can be stated as [43,45]

$$W_{\text{in}}(\xi) \rightarrow W_{\text{in}}(S_{\text{MZI}}^{-1}\xi) = W_{\text{out}}(\xi), \quad (8)$$

where $W_{\text{in}}(\xi) = W_{|\alpha\rangle}(\xi_1) \times W^{\text{NG}}(\xi_2)$ is the product of the Wigner distribution function of the coherent state (1) and NGSVSs (2). We employ parity detection on the output mode \hat{a}_2 as depicted in Fig. 1. The operator corresponding to parity detection is given by

$$\hat{\Pi}_{\hat{a}_2} = \exp(i\pi \hat{a}_2^\dagger \hat{a}_2) = (-1)^{\hat{a}_2^\dagger \hat{a}_2}. \quad (9)$$

To evaluate the average of the parity operator, we recall that the Wigner distribution function can be expressed as the average of the displaced parity operator [46]:

$$W(\xi) = \frac{1}{\pi^n} \text{Tr}[\hat{\rho} D(\xi) \hat{\Pi} D^\dagger(\xi)], \quad (10)$$

where n is the number of modes, $D(\xi) = \exp[i\hat{\xi}^T \Omega \xi]$ represents the displacement operator, and $\hat{\Pi} = \prod_{i=0}^n \exp(i\pi \hat{a}_i^\dagger \hat{a}_i)$ represents the parity operator. Hence, the average of the parity operator in terms of the Wigner distribution function turns out to be [47]

$$\langle \hat{\Pi}_{\hat{a}_2} \rangle = \pi \int d^2\xi_1 W_{\text{out}}(\xi_1, 0). \quad (11)$$

Upon substitution of Eq. (8) in Eq. (11), the calculation of the integral yields

$$\langle \hat{\Pi}_{\hat{a}_2} \rangle = \frac{\pi \hat{F}_1}{\sqrt{w_3 w_4}} \exp\left(\frac{\mathbf{u}^T M_4 \mathbf{u} + \mathbf{u}^T M_5 \mathbf{d} + \mathbf{d}^T M_6 \mathbf{d}}{-w_3 w_4}\right), \quad (12)$$

where $w_{3,4} = \cosh r \pm \tau \sinh r \cos \phi$ and $\mathbf{d} = (2d_x, 2d_p)^T$. Further, the matrices M_4 , M_5 , and M_6 are defined in Eqs. (C1), (C2), and (C3) of Appendix C. The phase uncertainty or sensitivity can be expressed as the following using the error propagation formula:

$$\Delta\phi = \frac{\sqrt{1 - \langle \hat{\Pi}_{\hat{a}_2} \rangle^2}}{|\partial \langle \hat{\Pi}_{\hat{a}_2} \rangle / \partial \phi|}. \quad (13)$$

The phase uncertainty is a function of the squeezing r of the SVS, displacement d_x and d_p of the coherent state, and the introduced unknown phase ϕ . Besides, the number of input photons m and the number of detected photons n can be appropriately chosen to perform different NG operations. One important advantage of our considered realistic model for the implementation of NG operations is that it allows us to consider the probability of different NG operations and consequently identify their effectiveness in phase estimation.

In the unit transmissivity limit ($\tau \rightarrow 1$) with $m = 0$, the phase sensitivity expression (13) reduces to that of ideal PSSVSs [32]. Similarly, in the unit transmissivity limit with $n = 0$, we obtain the phase sensitivity expression for ideal PASVSs [42]. Further, we obtain the phase sensitivity expression for the SVS using Eq. (13) in the limit $\tau \rightarrow 1$ with $m = n$ [33].

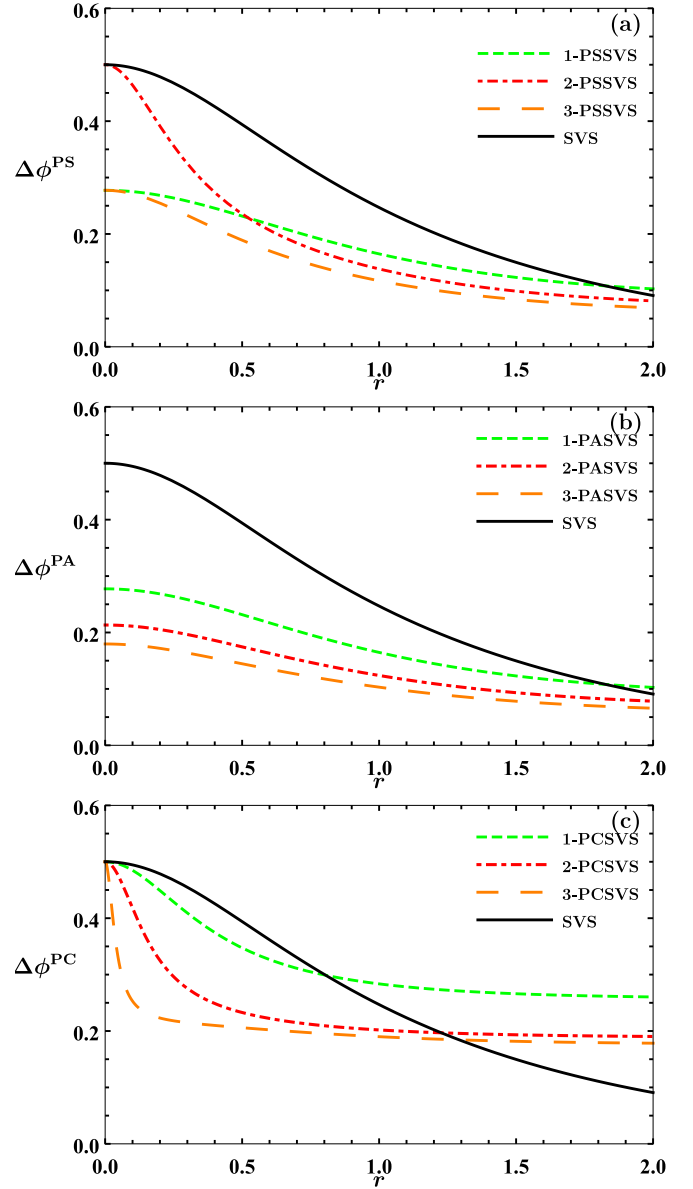


FIG. 2. Phase uncertainty $\Delta\phi$ as a function of the squeezing parameter r for NGSVSs. We have set the transmissivity of the beam splitter to be $\tau = 0.9$ for panels (a) and (b) and $\tau = 0.1$ for panel (c). Further, the coherent-state displacement has been taken to be $d_x = d_p = 2$ and phase $\phi = 0.01$ for all the panels.

III. PHASE SENSITIVITY ENHANCEMENT VIA NGSVSs

We now proceed to find out whether different NG operations on SVSs can enhance phase sensitivity in the MZI. To this end, we study the behavior of phase uncertainty ($\Delta\phi$) as a function of initial squeezing (r) of the SVS, transmissivity (τ) of the beam splitter used to perform NG operations, and magnitude of the total unknown phase (ϕ) introduced in the interferometer. In Fig. 2, we show the plot of $\Delta\phi$ as a function of squeezing, while other parameters are kept fixed.¹

¹In this paper, we set the displacement of the coherent state $d_x = d_p = 2$ for numerical analysis purposes.

As can be seen in Fig. 2(a), PSSVSs improve the phase sensitivity as compared to SVSs for almost the whole of the considered squeezing range. For 1-PSSVS, phase sensitivity improvement is not observed for $r \gtrsim 1.8$. The phase sensitivity via 2-PSSVS gets better than that of 1-PSSVS at a certain threshold squeezing. The phase sensitivity of 3-PSSVS is better than that of 1-PSSVS and 2-PSSVS.

An intriguing anomaly evident in Fig. 2(a) is the strange behavior exhibited by the PSSVSs, where 2-PSSVS fails to augment the phase sensitivity at $r = 0$, while 1-PSSVS and 3-PSSVS manifest such enhancement. This strange behavior can be explained by considering the following two factors: (i) if the input to the MZI is a coherent state combined with a Fock state ($|n\rangle$), then it has been established that the phase sensitivity improves with an increase in n [25], and (ii) in the limit of $r \rightarrow 0$, 1-PSSVS and 3-PSSVS become $|1\rangle$ whereas 2-PSSVS turns out to be $|0\rangle$. This can be seen by computing the Wigner function (2) in the $r \rightarrow 0$ limit. By taking into account the aforementioned points, we deduce that SVS and 2-PSSVS will yield the same phase sensitivity in the $r \rightarrow 0$ limit, while 1-PSSVS and 3-PSSVS will surpass the SVS in terms of phase sensitivity.

Moving to the PA operation, we observe that 1-PASVS significantly improves the phase sensitivity up to the squeezing value of $r \approx 1.8$. The phase sensitivity is enhanced further as more photons are added. Similarly, the PCSVSs yield better phase sensitivity as we catalyze more photons. However, the phase sensitivity is improved compared to the initial SVS for a much smaller range of the squeezing parameter, as shown in Fig. 2(c).

We now study the dependence of $\Delta\phi$ on the transmissivity while other parameters are kept fixed. The results are shown in Fig. 3. While phase sensitivity is maximized in the unit transmissivity limit for PSSVSs and PASVSs, phase sensitivity is maximized in the zero transmissivity limit for PCSVSs. While for 2-PSSVS, the phase sensitivity is enhanced beyond a threshold transmissivity, 1-PSSVS and 3-PSSVS improve phase sensitivity for the entire range of transmissivity. We obtain improved phase sensitivity for PASVSs for the entire range of transmissivity. In contrast, PCSVSs show improved phase sensitivity for a small range of low transmissivity.

The reason for these behaviors can be qualitatively explained by observing the photon number distribution (PND) of NGSVSs at different transmissivity values. For instance, we have shown the PND for PSSVSs at different transmissivity values in Fig. 8 in Appendix B. We first observe that for the SVS, the probability of the vacuum state $|0\rangle$ is significantly large (≈ 0.6). This contrasts with 1-PSSVS and 3-PSSVS where the vacuum state always has zero probability. This, along with the fact that nonzero Fock states yield better phase sensitivity, explains the enhancement in phase sensitivity when employing these two non-Gaussian states compared to SVSs. On the other hand, 2-PSSVS has a highly populated $|0\rangle$ state in the low-transmissivity regime. As the transmissivity increases, the PND is shifted to higher Fock states, which enhances the sensitivity. 2-PSSVS performs worse than the SVS in a low-transmissivity regime because the probability of $|0\rangle$ for 2-PSSVS is larger than that for the SVS. On increasing the transmissivity, the probability of the vacuum state decreases and becomes comparable with that of the SVS; therefore, their

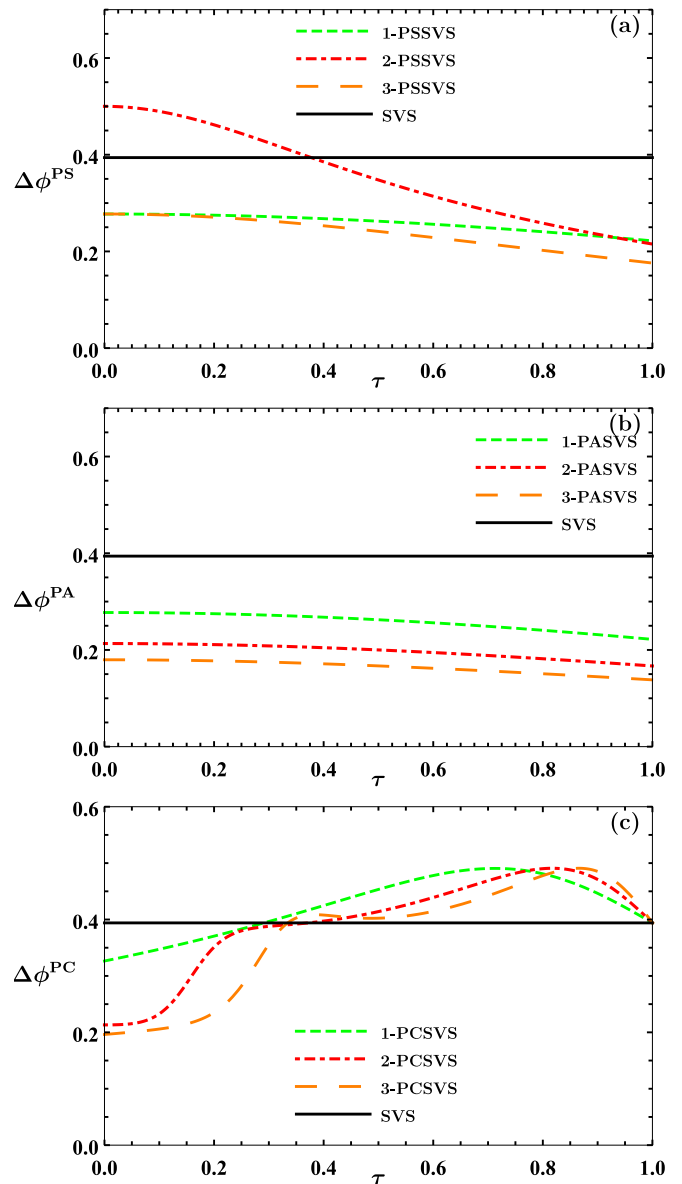


FIG. 3. Phase uncertainty $\Delta\phi$ as a function of the transmissivity of the beam splitter τ for NGSVSs. We have set the squeezing parameter $r = 0.5$ and the phase to be $\phi = 0.01$ for all the panels.

phase sensitivities also become comparable. With a further increase of transmissivity, the probability for $|0\rangle$ becomes even smaller for 2-PSSVS as compared to the SVS, and the sensitivity is further increased. In Fig. 4, we analyze the dependence of $\Delta\phi$ on the phase while other parameters are kept fixed. We notice a general trend that performing multiple NG operations results in the enhancement of phase sensitivity. However, a deviation is observed, where the 1-PS operation performs better than the 2-PS operation. Again these behaviors can be largely explained by a similar analysis of the PND for various non-Gaussian states as previously done. Figure 9 in Appendix B shows the PND for parameter values identical to Fig. 4. In the case of PASVSs (PCSVSs), an increase in the number of photons added (catalyzed) is accompanied by a shift of probability from lower to higher Fock states, thereby increasing the phase sensitivity. However, when we

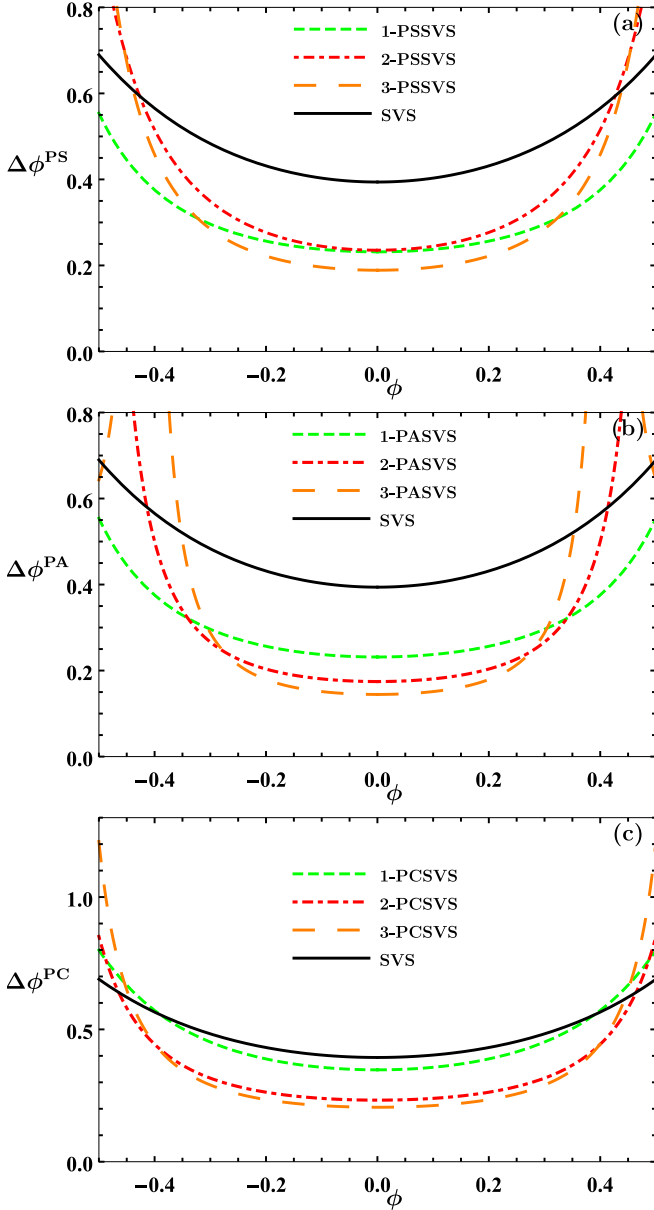


FIG. 4. Phase uncertainty $\Delta\phi$ as a function of the phase ϕ for NGSVSSs. We have set the transmissivity of the beam splitter to be $\tau = 0.9$ for panels (a) and (b) and $\tau = 0.1$ for panel (c). Further, the squeezing parameter has been set to be $r = 0.5$ for all the panels.

transition from odd-numbered PSSVSs (such as 1-PSSVS) to even-numbered PSSVSs (such as 2-PSSVS), the probability shifts from odd to even Fock states, leading to an increase in the probability of $|0\rangle$ for 2-PSSVS. As a result, the phase sensitivity is diminished for 2-PSSVS.

IV. OPTIMAL NG OPERATION FOR PHASE ESTIMATION

In the preceding section, we investigated the benefits of performing NG operations on the SVS for specific values of state parameters (r and τ) and phase ϕ . We now analyze the benefits of performing NG operations for a range of squeezing and transmissivity parameters at a fixed phase. This study enables us to get a good understanding of the effects of the

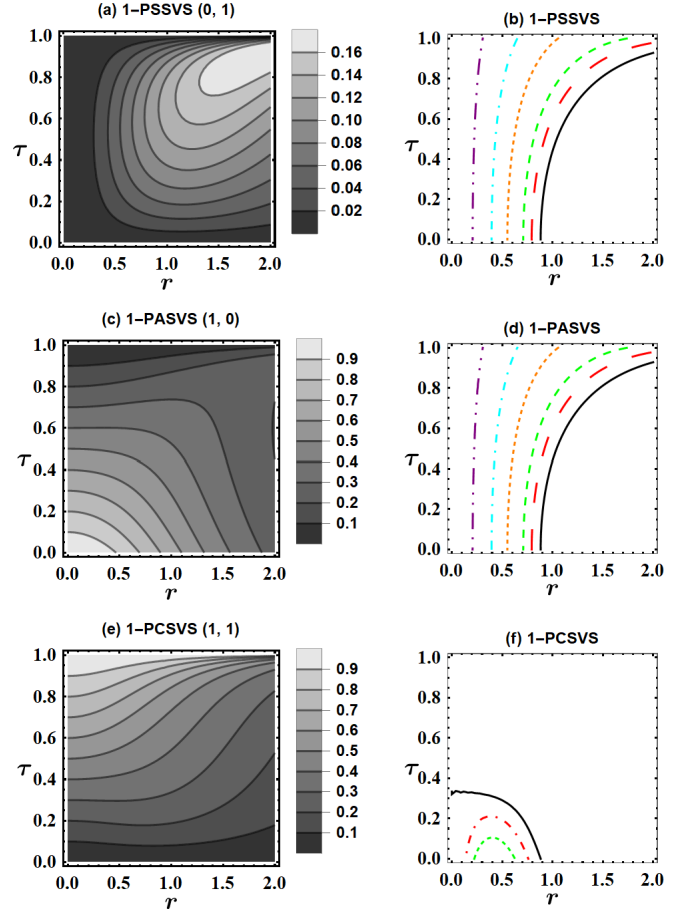


FIG. 5. Left panels depict the success probability as a function of the transmissivity τ and the squeezing parameter r for NGSVSSs. Right panels depict curves of fixed \mathcal{D}^{NG} , the difference of $\Delta\phi$ between SVS and NGSVSSs, as a function of τ and r . We have shown the values of the parameters (m, n) for different PSSVSs. The phase ϕ is taken to be 0.01. Solid black, large dashed red, dashed green, dotted orange, dot-dashed cyan, and double-dot-dashed purple curves represent $\mathcal{D}^{\text{NG}} = 0.00, 0.025, 0.05, 0.10, 0.15,$ and 0.20 , respectively.

NG operations. To this end, we consider the difference of $\Delta\phi$ between the SVS and NGSVSSs defined as follows:

$$\mathcal{D}^{\text{NG}} = \Delta\phi^{\text{SVS}} - \Delta\phi^{\text{NGSVSSs}}. \quad (14)$$

The region of state parameters (r and τ), where \mathcal{D}^{NG} turns out to be positive, signifies that NGSVSSs yield better phase sensitivity than the SVS.

We also consider the success probability of the NG operations and plot them alongside the \mathcal{D}^{NG} plots. The success probability signifies the fraction of successful NG operations and represents resource utilization. A careful comparison with the \mathcal{D}^{NG} plots enables us to qualitatively identify the optimal NG operation. In the left panels of Fig. 5, we draw the contours of the success probability in the $r - \tau$ space for different NG operations. We observe that the values of success probabilities reach to the range of 0.9 for both 1-PA and 1-PC operations. However, for the 1-PS operation, the success probability only reaches to the range of 0.16. For the 1-PS operation, the highest success probabilities are observed for high transmissivity and high values of squeezing. In contrast,

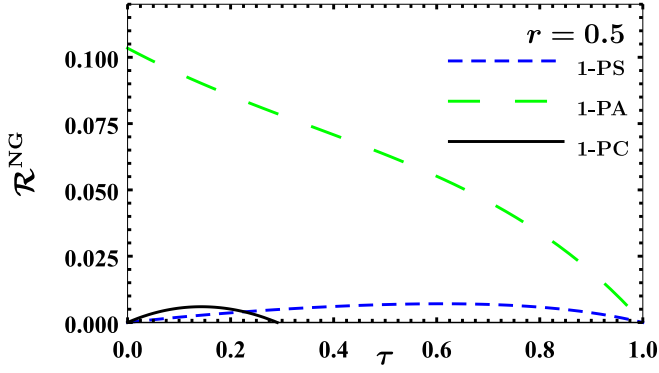


FIG. 6. Product $\mathcal{R}^{\text{NG}} = P^{\text{NG}} \times \mathcal{D}^{\text{NG}}$ as a function of the transmissivity τ for different NG states. The phase has been set as $\phi=0.01$ for all the cases.

for the 1-PA operation, the highest success probabilities are observed for low transmissivity and low values of squeezing. The highest success probabilities for the 1-PC operation are characterized by high values of transmissivity and by low to intermediate values of squeezing in our considered range.

The right panels of Fig. 5 show curves for different values of \mathcal{D}^{NG} ($= 0.00, 0.025, 0.05, 0.10, 0.15, 0.20$) corresponding to 1-PSSVS, 1-PASVS, and 1-PCSVS. For 1-PSSVS and 1-PASVS, the region of positive \mathcal{D}^{NG} is obtained for the squeezing range $r \in (0, 1)$ for small values of transmissivity. As the transmissivity increases, the advantageous squeezing range also increases. For 1-PCSVS, the region of positive \mathcal{D}^{NG} is observed for low transmissivity and low values of squeezing.

In order to qualitatively find the most optimal NG state, we consider following two main factors: the overlap of positive regions of \mathcal{D}^{NG} with regions of high success probability, and the magnitude of the highest success probability achieved. Clearly, 1-PCSVS is out of the picture as the areas of high success probabilities do not overlap with the region with positive values of \mathcal{D}^{NG} . The next scope of comparison is between 1-PSSVS and 1-PASVS where both have a considerable overlap of positive \mathcal{D}^{NG} and high success probabilities. Here, 1-PASVS turns out to be the most optimal state as the magnitude of high success probabilities (≈ 0.9) is much greater than that of 1-PSSVS (≈ 0.16).

To see this comparison in a much more quantitative manner, we consider the product $\mathcal{R}^{\text{NG}} = P^{\text{NG}} \times \mathcal{D}^{\text{NG}}$. Here we trade-off between P^{NG} and \mathcal{D}^{NG} by adjusting the transmissivity for a given squeezing to maximize the product. The optimal state renders this product maximum. To that end, we numerically study the dependence of the product \mathcal{R}^{NG} on the transmissivity at a fixed squeezing for different NG states in Fig. 6. The results reveal that 1-PASVS performs way better than other considered states when the success probability is taken into consideration. However, we notice that the best performance is achieved at $\tau = 0$, which cannot be achieved in an experiment. The best experimental strategy would be to work in a low-transmissivity regime such as $\tau = 0.01$. We also note that 1-PASVS becomes $|1\rangle$ in the limit $\tau \rightarrow 0$. Therefore, one could use the coherent state combined with $|1\rangle$ as the input state to obtain similar phase sensitivity.

V. CONCLUSION

In this paper, we investigated the advantages offered by non-Gaussian operations in phase estimation using a parity-detection-based MZI, with a coherent state and NGSVSs as the two inputs. We considered the realistic scheme for implementing three different NG operations, namely, PS, PA, and PC, on the SVS state. We derived the Wigner function for the three corresponding NGSVSs, i.e., PSSVSs, PASVSs, and PCSVSs. The Wigner function is then used to derive the phase sensitivity of a parity-detection-based MZI. The investigation of the phase sensitivity reveals that all the three NG operations can enhance the phase sensitivity for suitable choices of different NG operations into account.

The results show that the optimal operation for phase estimation is single-photon addition on the SVS. This is because the parameter range of high success probability for a single PA operation and the large enhancement in the phase sensitivity by 1-PASVS coincide [Fig. 5(b)]. We would like to stress that our scheme for NG state generation can be realized with currently available technologies and, therefore, is of direct relevance to the experimental community. In contrast, Refs. [32,42] have considered photon annihilation and creation operator for the implementation of PS and PA operations, which are nonphysical. In addition, our considered figure of merit also enables us to find optimal squeezing and transmissivity parameters.

Our study can be extended in several directions. Lang and Caves have reported that for an interferometer with a coherent state being one input and the other being constrained by the average photon number, the optimal state to inject through the second input is the squeezed vacuum state (SVS) [8]. In a similar spirit, Ref. [42] has compared the phase sensitivity of ideal PSSVSs and PASVSs with a constraint on the average photon number. It would be interesting to compare the phase sensitivity of NG states, including PCSVSs generated by a realistic scheme under such constraints. Further, we can also explore different measurement-based MZI, such as intensity measurement [48] and homodyne measurement [49]. Furthermore, such an analysis involving realistic NG operation schemes can be extended to different classes of states, such as displaced Fock states [50].

ACKNOWLEDGMENT

We thank R. Choudhary for reading the final version of the manuscript. C.K. acknowledges the financial support from DST/ICPS/QuST/Theme-1/2019/General Project No. Q-68.

APPENDIX A: CALCULATION OF WIGNER DISTRIBUTION FUNCTION FOR NGSVSs

In this Appendix, we provide a detailed and stepwise calculation of the Wigner distribution function for the NGSVSs. The scheme for the generation of the NGSVSs is illustrated in Fig. 7. We start with a single-mode SVS which can be written as

$$|\text{SVS}\rangle = \mathcal{U}(S(r))|0\rangle, \quad (\text{A1})$$

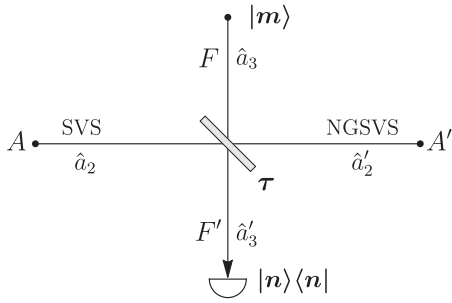


FIG. 7. Schematic representation of photon subtraction, addition, and catalysis operations on SVSs. A beam splitter of transmissivity τ is used to mix the SVS and the ancilla Fock state $|m\rangle$. Detection of n photons in the ancilla output mode F' heralds the generation of the NGSVSs.

where $\mathcal{U}(S(r)) = \exp[r(\hat{a}_2^2 - \hat{a}_2^{\dagger 2})/2]$ is the single-mode squeezing operator. This is a Gaussian state with zero mean and the following covariance matrix:

$$V = \frac{1}{2} \begin{pmatrix} e^{-2r} & 0 \\ 0 & e^{2r} \end{pmatrix}. \quad (\text{A2})$$

The Wigner distribution function for the SVS turns out to be [43]

$$W(\xi_2) = \pi^{-1} \exp(-e^{-2r} q_2^2 - e^{2r} p_2^2), \quad (\text{A3})$$

where $\xi_2 = (q_2, p_2)^T$. As shown in Fig. 7, the SVS in mode A is combined with the Fock state $|m\rangle$ in the ancilla mode F using a beam splitter of transmissivity τ . The state of the two-mode system before the beam-splitter transformation can be represented by its Wigner distribution function as follows:

$$W_{AF}(\xi) = W_A(\xi_2) W_{|m\rangle}(\xi_3), \quad (\text{A4})$$

where the Wigner distribution function of a Fock state $|m\rangle$ is given by

$$W_{|m\rangle}(q, p) = \frac{(-1)^m}{\pi} \exp(-q^2 - p^2) L_m[2(q^2 + p^2)], \quad (\text{A5})$$

with $L_m\{\bullet\}$ being the Laguerre polynomial of the n th order. The action of the beam-splitter operation on the phase-space variables $(\xi_2, \xi_3)^T$ is given by the symplectic matrix

$$B_{AF}(\tau) = \begin{pmatrix} \sqrt{\tau} \mathbb{1}_2 & \sqrt{1-\tau} \mathbb{1}_2 \\ -\sqrt{1-\tau} \mathbb{1}_2 & \sqrt{\tau} \mathbb{1}_2 \end{pmatrix}. \quad (\text{A6})$$

The beam splitter entangles the two modes, and the corresponding Wigner distribution function of the entangled state can be written as

$$W_{A'F'}(\xi) = W_{AF}[B_{AF}(\tau)^{-1}\xi]. \quad (\text{A7})$$

We now perform a conditional measurement on the ancilla mode of the output state F' using a photon-number-resolving detector. Detection of n photons corresponds to successful implementation of the NG operation on the SVS. The un-normalized Wigner distribution function of the NGSVSs will be

$$\tilde{W}_{A'}^{\text{NG}}(\xi_2) = 2\pi \int d^2 \xi_3 W_{A'F'}(\xi_2, \xi_3) \times \underbrace{W_{|n\rangle}(\xi_3)}_{\text{Projection on } |n\rangle\langle n|}. \quad (\text{A8})$$

The cases $m < n$ and $m > n$ correspond to the implementation of PS and PA operations on the SVS, respectively, while $m = n$ corresponds to the implementation of the PC operation on the SVS. PS and PA operations on the SVS produce PSSVSs and PASVSs, respectively. Similarly, the PC operation on the SVS produces PCSVSs. The states generated by performing these NG operations are NG. The following identity for the Laguerre polynomials can be used to transform the integrand of Eq. (A8) into a Gaussian function:

$$L_n[2(q^2 + p^2)] = \hat{D} \exp\left[\frac{st}{2} + s(q + ip) - t(q - ip)\right], \quad (\text{A9})$$

where the differential operator \hat{D} is given by

$$\hat{D} = \frac{2^n}{n!} \frac{\partial^n}{\partial s^n} \frac{\partial^n}{\partial t^n} \{\bullet\}_{s=t=0}. \quad (\text{A10})$$

The transformed expression (A8) can be readily integrated to obtain

$$\tilde{W}_{A'}^{\text{NG}}(\xi_2) = \frac{\hat{F}_1}{\sqrt{w_1 w_2}} \exp\left(\frac{w_1^2 q_2^2 + w_2^2 p_2^2 + \mathbf{u}^T M_1 \mathbf{u} + \mathbf{u}^T M_2}{-w_1 w_2}\right), \quad (\text{A11})$$

where $w_{1,2} = \cosh r \pm \tau \sinh r$, the column vector \mathbf{u} is defined as $\mathbf{u} = (u_1, v_1, u_2, v_2)^T$, and the differential operator \hat{F}_1 is defined as

$$\hat{F}_1 = \frac{(-2)^{m+n}}{\pi m! n!} \frac{\partial^m}{\partial u_1^m} \frac{\partial^m}{\partial v_1^m} \frac{\partial^n}{\partial u_2^n} \frac{\partial^n}{\partial v_2^n} \{\bullet\}_{\substack{u_1=v_1=0 \\ u_2=v_2=0}}. \quad (\text{A12})$$

Further, the matrix M_1 is given by

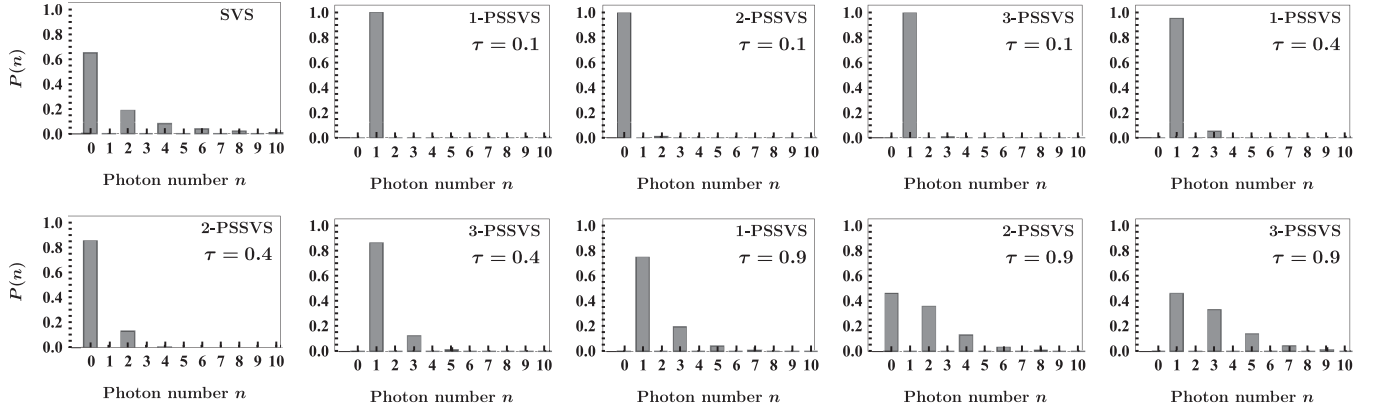
$$M_1 = \frac{1}{4} \begin{pmatrix} \alpha \beta t'^2 t^2 & -\beta^2 t'^2 & \alpha \beta t'^2 t & \alpha^2 t'^2 t + t \\ -\beta^2 t'^2 & \alpha \beta t'^2 t^2 & \alpha^2 t'^2 t + t & \alpha \beta t'^2 t \\ \alpha \beta t'^2 t & \alpha^2 t'^2 t + t & \alpha \beta t'^2 & -\alpha^2 t'^2 t^2 \\ \alpha^2 t'^2 t + t & \alpha \beta t'^2 & -\alpha^2 t'^2 t^2 & \alpha \beta t'^2 \end{pmatrix}, \quad (\text{A13})$$

where $t = \sqrt{\tau}$, $t' = \sqrt{1-\tau}$, $\alpha = \sinh r$, and $\beta = \cosh r$. The matrix M_2 is given by

$$M_2 = \begin{pmatrix} -\beta t'(q_2 w_1 + i p_2 w_2) \\ \beta t'(q_2 w_1 - i p_2 w_2) \\ -\alpha t'(q_2 w_1 - i p_2 w_2) \\ \alpha t'(q_2 w_1 + i p_2 w_2) \end{pmatrix}. \quad (\text{A14})$$

The probability of successful generation of NG states can be evaluated by integrating the un-normalized Wigner distribution function of the NGSVSs (A11):

$$P^{\text{NG}} = \int d^2 \xi_2 \tilde{W}_{A'}^{\text{NG}}(\xi_2) = \frac{\pi \hat{F}_1}{\sqrt{w_1 w_2}} \exp\left(\frac{\mathbf{u}^T M_3 \mathbf{u}}{-4w_1 w_2}\right), \quad (\text{A15})$$

FIG. 8. Photon number distribution of the SVS and PSSVSs. We have set $r = 0.5$.

where the matrix M_3 is represented as below:

$$M_3 = \begin{pmatrix} \alpha\beta t'^2 t^2 & \beta^2 t'^2 & \alpha\beta t'^2 t w_0^2 & t + \alpha^2 t'^2 t \\ \beta^2 t'^2 & \alpha\beta t'^2 t^2 & t + \alpha^2 t'^2 t & \alpha\beta t'^2 t w_0^2 \\ \alpha\beta t'^2 t w_0^2 & t + \alpha^2 t'^2 t & \alpha\beta t'^2 & \alpha^2 t'^2 t^2 \\ t + \alpha^2 t'^2 t & \alpha\beta t'^2 t w_0^2 & \alpha^2 t'^2 t^2 & \alpha\beta t'^2 \end{pmatrix}, \quad (\text{A16})$$

where $w_0 = e^{-2r}(w_2 + t'^2 \alpha^2)/(w_1 - t'^2 \alpha^2)$. The normalized Wigner distribution function $W_{A'}^{\text{NG}}$ of the NGSVSs can be written as follows:

$$W_{A'}^{\text{NG}}(\xi_2) = (P^{\text{NG}})^{-1} \tilde{W}_{A'}^{\text{NG}}(\xi_2). \quad (\text{A17})$$

APPENDIX B: PHOTON NUMBER DISTRIBUTION OF NGSVS

The effect of NG operations on the SVS can be easily seen through the change in the photon number distribution (PND). The PND or the probability of finding n photons can be calculated as

$$P(n) = 2\pi \int d^2 \xi_2 W^{\text{NG}}(\xi_2) W_{|n\rangle}(\xi_2). \quad (\text{B1})$$

In order to explain some of the intriguing behavior shown by NGSVSs (in the main text), we show the PND for some specific parameter values. For instance, Fig. 8 shows the PND for the three PSSVSs at different transmissivity values. The squeezing value is set at 0.5 for all these states. The PND for

the SVS is also included for comparison. Similarly, Fig. 9 shows the PND for parameter values identical to those in Fig. 4.

APPENDIX C: MATRICES APPEARING IN THE AVERAGE OF PARITY OPERATOR

Here we provide the expressions of the matrices M_4 , M_5 , and M_6 which appear in the average of parity operator (12):

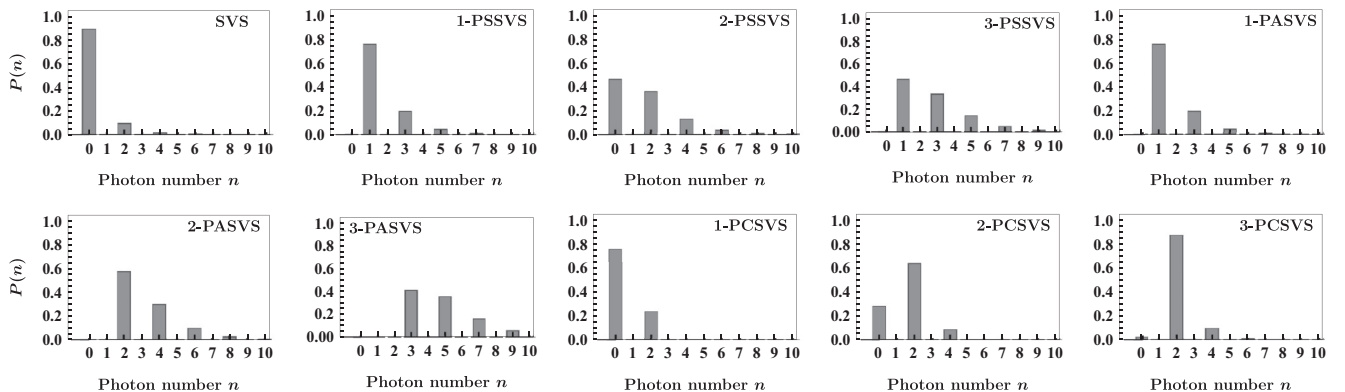
$$M_4 = \begin{pmatrix} \alpha\beta\gamma^2 t'^2 t^2 & -\beta^2 \gamma t'^2 & \alpha\beta\gamma t'^2 t & t w_3 w_4 \\ -\beta^2 \gamma t'^2 & \alpha\beta\gamma^2 t'^2 t^2 & t w_3 w_4 & \alpha\beta\gamma t'^2 t \\ \alpha\beta\gamma t'^2 t & t w_3 w_4 & \alpha\beta t'^2 & -\alpha^2 \gamma t'^2 t^2 \\ t w_3 w_4 & \alpha\beta\gamma t'^2 t & -\alpha^2 \gamma t'^2 t^2 & \alpha\beta t'^2 \end{pmatrix}, \quad (\text{C1})$$

where $\gamma = \cos \phi$ and $\delta = \sin \phi$. Further,

$$M_5 = \begin{pmatrix} \beta\delta t' w_3 & i\beta\delta t' w_4 \\ -\beta\delta t' w_3 & i\beta\delta t' w_4 \\ \alpha\delta t' w_3 & -i\alpha\delta t' w_4 \\ -\alpha\delta t' w_3 & -i\alpha\delta t' w_4 \end{pmatrix} \quad (\text{C2})$$

and

$$M_6 = \sin^2\left(\frac{\phi}{2}\right) \begin{pmatrix} w_3 w_1 & 0 \\ 0 & w_4 w_2 \end{pmatrix}. \quad (\text{C3})$$

FIG. 9. Photon number distribution of NGSVSs. We have set $r = 0.5$ and transmissivity of the beam splitter to be $\tau = 0.9$ for PS and PA and $\tau = 0.1$ for PC.

- [1] J. P. Dowling, Quantum optical metrology—the lowdown on high-N00N states, *Contemp. Phys.* **49**, 125 (2008).
- [2] V. Giovannetti, S. Lloyd, and L. Maccone, Advances in quantum metrology, *Nat. Photon.* **5**, 222 (2011).
- [3] C. M. Caves, Quantum-mechanical noise in an interferometer, *Phys. Rev. D* **23**, 1693 (1981).
- [4] A. N. Boto, P. Kok, D. S. Abrams, S. L. Braunstein, C. P. Williams, and J. P. Dowling, Quantum Interferometric Optical Lithography: Exploiting Entanglement to Beat the Diffraction Limit, *Phys. Rev. Lett.* **85**, 2733 (2000).
- [5] V. Giovannetti, S. Lloyd, and L. Maccone, Quantum-enhanced measurements: Beating the standard quantum limit, *Science* **306**, 1330 (2004).
- [6] H. F. Hofmann and T. Ono, High-photon-number path entanglement in the interference of spontaneously down-converted photon pairs with coherent laser light, *Phys. Rev. A* **76**, 031806(R) (2007).
- [7] P. M. Anisimov, G. M. Raterman, A. Chiruvelli, W. N. Plick, S. D. Huver, H. Lee, and J. P. Dowling, Quantum Metrology with Two-Mode Squeezed Vacuum: Parity Detection Beats the Heisenberg Limit, *Phys. Rev. Lett.* **104**, 103602 (2010).
- [8] M. D. Lang and C. M. Caves, Optimal Quantum-Enhanced Interferometry Using a Laser Power Source, *Phys. Rev. Lett.* **111**, 173601 (2013).
- [9] H. Kwon, K. C. Tan, T. Volkoff, and H. Jeong, Nonclassicality as a Quantifiable Resource for Quantum Metrology, *Phys. Rev. Lett.* **122**, 040503 (2019).
- [10] H. Vahlbruch, M. Mehmert, K. Danzmann, and R. Schnabel, Detection of 15 dB Squeezed States of Light and Their Application for the Absolute Calibration of Photoelectric Quantum Efficiency, *Phys. Rev. Lett.* **117**, 110801 (2016).
- [11] T. Opatrny, G. Kurizki, and D.-G. Welsch, Improvement on teleportation of continuous variables by photon subtraction via conditional measurement, *Phys. Rev. A* **61**, 032302 (2000).
- [12] A. Kitagawa, M. Takeoka, M. Sasaki, and A. Chefles, Entanglement evaluation of non-Gaussian states generated by photon subtraction from squeezed states, *Phys. Rev. A* **73**, 042310 (2006).
- [13] F. Dell’Anno, S. De Siena, L. Albano, and F. Illuminati, Continuous-variable quantum teleportation with non-Gaussian resources, *Phys. Rev. A* **76**, 022301 (2007).
- [14] Y. Yang and F.-L. Li, Entanglement properties of non-gaussian resources generated via photon subtraction and addition and continuous-variable quantum-teleportation improvement, *Phys. Rev. A* **80**, 022315 (2009).
- [15] S. Wang, L.-L. Hou, X.-F. Chen, and X.-F. Xu, Continuous-variable quantum teleportation with non-Gaussian entangled states generated via multiple-photon subtraction and addition, *Phys. Rev. A* **91**, 063832 (2015).
- [16] X.-X. Xu, Enhancing quantum entanglement and quantum teleportation for two-mode squeezed vacuum state by local quantum-optical catalysis, *Phys. Rev. A* **92**, 012318 (2015).
- [17] L. Hu, Z. Liao, and M. S. Zubairy, Continuous-variable entanglement via multiphoton catalysis, *Phys. Rev. A* **95**, 012310 (2017).
- [18] C. Kumar and S. Arora, Success probability and performance optimization in non-Gaussian continuous-variable quantum teleportation, *Phys. Rev. A* **107**, 012418 (2023).
- [19] P. Huang, G. He, J. Fang, and G. Zeng, Performance improvement of continuous-variable quantum key distribution via photon subtraction, *Phys. Rev. A* **87**, 012317 (2013).
- [20] H.-X. Ma, P. Huang, D.-Y. Bai, S.-Y. Wang, W.-S. Bao, and G.-H. Zeng, Continuous-variable measurement-device-independent quantum key distribution with photon subtraction, *Phys. Rev. A* **97**, 042329 (2018).
- [21] Y. Guo, W. Ye, H. Zhong, and Q. Liao, Continuous-variable quantum key distribution with non-Gaussian quantum catalysis, *Phys. Rev. A* **99**, 032327 (2019).
- [22] W. Ye, H. Zhong, Q. Liao, D. Huang, L. Hu, and Y. Guo, Improvement of self-referenced continuous-variable quantum key distribution with quantum photon catalysis, *Opt. Express* **27**, 17186 (2019).
- [23] L. Hu, M. Al-amri, Z. Liao, and M. S. Zubairy, Continuous-variable quantum key distribution with non-Gaussian operations, *Phys. Rev. A* **102**, 012608 (2020).
- [24] S. L. Zhang, J. S. Guo, W. S. Bao, J. H. Shi, C. H. Jin, X. B. Zou, and G. C. Guo, Quantum illumination with photon-subtracted continuous-variable entanglement, *Phys. Rev. A* **89**, 062309 (2014).
- [25] R. Birrittella, J. Mimih, and C. C. Gerry, Multiphoton quantum interference at a beam splitter and the approach to Heisenberg-limited interferometry, *Phys. Rev. A* **86**, 063828 (2012).
- [26] R. Carranza and C. C. Gerry, Photon-subtracted two-mode squeezed vacuum states and applications to quantum optical interferometry, *J. Opt. Soc. Am. B* **29**, 2581 (2012).
- [27] D. Braun, P. Jian, O. Pinel, and N. Treps, Precision measurements with photon-subtracted or photon-added Gaussian states, *Phys. Rev. A* **90**, 013821 (2014).
- [28] Y. Ouyang, S. Wang, and L. Zhang, Quantum optical interferometry via the photon-added two-mode squeezed vacuum states, *J. Opt. Soc. Am. B* **33**, 1373 (2016).
- [29] H. Zhang, W. Ye, C. Wei, Y. Xia, S. Chang, Z. Liao, and L. Hu, Improved phase sensitivity in a quantum optical interferometer based on multiphoton catalytic two-mode squeezed vacuum states, *Phys. Rev. A* **103**, 013705 (2021).
- [30] C. Kumar, Rishabh, and S. Arora, Realistic non-Gaussian-operation scheme in parity-detection-based Mach-Zehnder quantum interferometry, *Phys. Rev. A* **105**, 052437 (2022).
- [31] C. Kumar, Rishabh, and S. Arora, Enhanced phase estimation in parity detection based Mach-Zehnder interferometer using non-Gaussian two-mode squeezed thermal input state, *Ann. Phys.* **2023**, 2300117 (2023).
- [32] R. Birrittella and C. C. Gerry, Quantum optical interferometry via the mixing of coherent and photon-subtracted squeezed vacuum states of light, *J. Opt. Soc. Am. B* **31**, 586 (2014).
- [33] K. P. Seshadreesan, P. M. Anisimov, H. Lee, and J. P. Dowling, Parity detection achieves the Heisenberg limit in interferometry with coherent mixed with squeezed vacuum light, *New J. Phys.* **13**, 083026 (2011).
- [34] A. I. Lvovsky, H. Hansen, T. Aichele, O. Benson, J. Mlynek, and S. Schiller, Quantum State Reconstruction of the Single-Photon Fock State, *Phys. Rev. Lett.* **87**, 050402 (2001).
- [35] A. Zavatta, S. Viciani, and M. Bellini, Tomographic reconstruction of the single-photon Fock state by high-frequency homodyne detection, *Phys. Rev. A* **70**, 053821 (2004).
- [36] S. R. Huisman, N. Jain, S. A. Babichev, F. Vewinger, A. N. Zhang, S. H. Youn, and A. I. Lvovsky, Instant single-photon Fock state tomography, *Opt. Lett.* **34**, 2739 (2009).

- [37] A. Ourjoumtsev, R. Tualle-Brouiri, and P. Grangier, Quantum Homodyne Tomography of a Two-Photon Fock State, *Phys. Rev. Lett.* **96**, 213601 (2006).
- [38] M. Cooper, L. J. Wright, C. Söller, and B. J. Smith, Experimental generation of multi-photon Fock states, *Opt. Express* **21**, 5309 (2013).
- [39] A. E. Lita, A. J. Miller, and S. W. Nam, Counting near-infrared single-photons with 95% efficiency, *Opt. Express* **16**, 3032 (2008).
- [40] F. Marsili, V. B. Verma, J. A. Stern, S. Harrington, A. E. Lita, T. Gerrits, I. Vayshenker, B. Baek, M. D. Shaw, R. P. Mirin, and S. W. Nam, Detecting single infrared photons with 93% system efficiency, *Nat. Photon.* **7**, 210 (2013).
- [41] I. Esmail Zadeh, J. W. N. Los, R. B. M. Gourgues, V. Steinmetz, G. Bulgarini, S. M. Dobrovolskiy, V. Zwiller, and S. N. Dorenbos, Single-photon detectors combining high efficiency, high detection rates, and ultra-high timing resolution, *APL Photon.* **2**, 111301 (2017).
- [42] S. Wang, X. Xu, Y. Xu, and L. Zhang, Quantum interferometry via a coherent state mixed with a photon-added squeezed vacuum state, *Opt. Commun.* **444**, 102 (2019).
- [43] C. Weedbrook, S. Pirandola, R. García-Patrón, N. J. Cerf, T. C. Ralph, J. H. Shapiro, and S. Lloyd, Gaussian quantum information, *Rev. Mod. Phys.* **84**, 621 (2012).
- [44] B. Yurke, S. L. McCall, and J. R. Klauder, Su(2) and SU(1,1) interferometers, *Phys. Rev. A* **33**, 4033 (1986).
- [45] Arvind, B. Dutta, N. Mukunda, and R. Simon, The real symplectic groups in quantum mechanics and optics, *Pramana* **45**, 471 (1995).
- [46] A. Royer, Wigner function as the expectation value of a parity operator, *Phys. Rev. A* **15**, 449 (1977).
- [47] R. J. Birrittella, P. M. Alsing, and C. C. Gerry, The parity operator: Applications in quantum metrology, *AVS Quantum Sci.* **3**, 014701 (2021).
- [48] S. Ataman, A. Preda, and R. Ionicioiu, Phase sensitivity of a Mach-Zehnder interferometer with single-intensity and difference-intensity detection, *Phys. Rev. A* **98**, 043856 (2018).
- [49] R. S. Bondurant and J. H. Shapiro, Squeezed states in phase-sensing interferometers, *Phys. Rev. D* **30**, 2548 (1984).
- [50] P. Malpani, K. Thapliyal, N. Alam, A. Pathak, V. Narayanan, and S. Banerjee, Quantum phase properties of photon added and subtracted displaced Fock states, *Ann. Phys.* **531**, 1900141 (2019).